

## Richtmyer-Meshkov instabilities in stratified fluids

Karnig O. Mikaelian

Lawrence Livermore National Laboratory, University of California, Livermore, California 94550

(Received 30 January 1984; revised manuscript received 21 August 1984)

We present an analytic theory of Richtmyer-Meshkov instabilities in an arbitrary number  $N$  of stratified fluids subjected to a shock. Following our earlier work on Rayleigh-Taylor instabilities, the theory assumes incompressible flow in which a shock is treated as an impulsive acceleration. We discuss the special cases  $N=2$  and  $N=3$ , and illustrate both Rayleigh-Taylor and Richtmyer-Meshkov instabilities by examples patterned after inertial-confinement-fusion implosions.

### I. INTRODUCTION

The Rayleigh-Taylor<sup>1,2</sup> (RT) instability occurs in systems undergoing a constant acceleration, while the Richtmyer-Meshkov<sup>3,4</sup> (RM) instability occurs in systems which have been impulsively accelerated by a shock. For both types of instabilities the classical case is a system of two semi-infinite fluids of densities  $\rho_1$  and  $\rho_2$ , with perturbations of wavelength  $\lambda$  at their common interface. If the acceleration is constant (RT case), then these perturbations grow exponentially in time,

$$\eta/\eta(0) = e^{\gamma\tau}, \quad \gamma = \sqrt{gkA}, \quad (1)$$

(RT case) where  $g$  is the acceleration directed from  $\rho_1$  to  $\rho_2$ ,  $k = 2\pi/\lambda$ , and  $A = (\rho_2 - \rho_1)/(\rho_2 + \rho_1)$  is the Atwood number. If the acceleration is impulsive (RM case), then the perturbations grow linearly in time,

$$\eta/\eta(0) = 1 + \gamma\tau, \quad \gamma = \Delta v k A, \quad (2)$$

(RM case) where  $\Delta v$  is the jump velocity caused by the passage of a shock from  $\rho_1$  to  $\rho_2$ . In Eqs. (1) and (2)  $\eta$  is the amplitude of the sinusoidal perturbations and  $\tau$  stands for time.

Equation (2), derived by Richtmyer,<sup>3</sup> is based on the same assumptions that go into the derivation of the classical RT result, Eq. (1). Both equations are valid only in the small amplitude, or linear, regime, i.e.,  $\eta \ll \lambda$ . The fluids are assumed to be incompressible with no viscosity or surface tension, and heat transfer is neglected. Detailed numerical calculations by Richtmyer<sup>3</sup> showed good agreement with Eq. (2) if the instantaneous reduction in amplitude due to shock compression was taken into account. Experiments by Meshkov<sup>4</sup> confirmed the prediction that amplitudes grow linearly with time after the passage of a shock. As the amplitude grows, the linear approximation is no longer valid: turbulent mixing takes place. Subsequent experiments<sup>5</sup> observed this mixing and a semiempirical model was developed.

Recently we generalized<sup>6</sup> the results of the classical RT instability to a system of an arbitrary number  $N$  of stratified fluids (see Fig. 1). In this paper we derive the corresponding equations for the RM instability. The classical results, Eqs. (1) and (2), will be special cases given by  $N = 2$ .

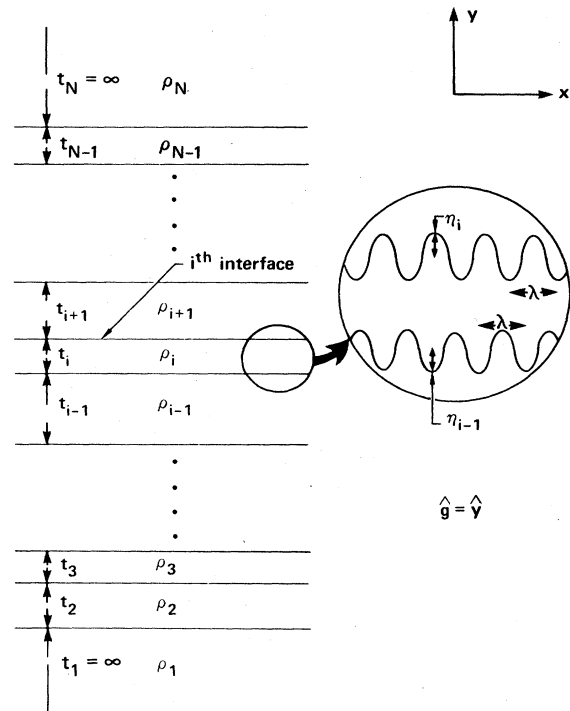


FIG. 1.  $N$  fluid layers of density  $\rho_1, \dots, \rho_N$  and thickness  $t_1, \dots, t_N$  which are stacked in the direction of acceleration  $\hat{g} = \hat{y}$ , where  $g$  is constant for Rayleigh-Taylor and  $g = \Delta v \delta(\tau - \tau_s)$  for Richtmyer-Meshkov instabilities. Unperturbed densities are uniform in the  $x$  and  $z$  directions and vary only in the  $y$  direction. The amplitude of sinusoidal perturbations at each interface  $i$  is denoted by  $\eta_i$ . The wavelength of the perturbations is  $\lambda$ .

## II. DERIVATION OF THE GENERAL EQUATION

Figure 1 shows the system and some of our notation:  $N$  fluid layers of densities  $\rho_1, \rho_2, \dots, \rho_N$  and thicknesses  $t_1, t_2, \dots, t_N$ . There are  $N-1$  interfaces and  $\eta_i$  is the amplitude of perturbations (of wavelength  $\lambda$ ) at the interface between  $\rho_i$  and  $\rho_{i+1}$ .

We showed in Ref. 6 that there are  $N-1$  eigenvalues  $\gamma_l$  and associated eigenfunctions  $W^l$  obtained by solving

$$\underline{M}W = \frac{gk}{\gamma^2} W, \quad (3)$$

where  $\underline{M}$  is a  $(N-1) \times (N-1)$  tridiagonal dimensionless matrix, the elements of which depend only on  $kt_i$  and the ratios  $\rho_i/\rho_{i+1}$ . Expanding in terms of these eigenfunctions we derived<sup>7</sup> a general equation which describes how the amplitude  $\eta_i$  at interface  $i$  evolves in time:

$$\begin{aligned} \eta_i(\tau) = & \sum_{l=1}^{N-1} \sum_{j=1}^{N-1} W(i,l)W^{-1}(l,j) \\ & \times \{ \eta_j(0) \cosh(\gamma_l \tau) + [\dot{\eta}_j(0)/\gamma_l] \\ & \times \sinh(\gamma_l \tau) \}, \end{aligned} \quad (4)$$

where  $W(i,l)$  and  $W^{-1}(l,j)$  are, respectively, the  $(i,l)$ th and  $(l,j)$ th element of the matrix  $\underline{W}$  and its inverse  $\underline{W}^{-1}$ .

To obtain the corresponding equation for the RM case, we use a technique similar to the one used by Richtmyer<sup>3</sup> in obtaining Eq. (2). From Eq. (4),

$$\begin{aligned} \frac{d^2 \eta_i(\tau)}{d\tau^2} = & g \sum_{l=1}^{N-1} \sum_{j=1}^{N-1} \Gamma_l^2 W(i,l)W^{-1}(l,j) \\ & \times \{ \eta_j(0) \cosh(\gamma_l \tau) + [\dot{\eta}_j(0)/\gamma_l] \\ & \times \sinh(\gamma_l \tau) \}, \end{aligned} \quad (5)$$

where we have defined  $\gamma_l^2 = g \Gamma_l^2$ . With this definition,  $\Gamma_l$  is independent of  $g$  since  $\gamma_l^2$  is proportional to  $g$  [see Eq. (3)].

Following Ref. 3 we represent a shock by an impulsive acceleration, i.e., let  $g = \Delta v \delta(\tau - \tau_s)$ , where  $\tau_s$  is the shock arrival time. This implies that  $g = 0$  immediately before ( $\tau < \tau_s$ ) and immediately after ( $\tau > \tau_s$ ) the shock. Actually we can treat the case where the shock is immediately preceded and/or followed by a finite acceleration (see Sec. IV), but in this section we treat the case of an isolated shock for clarity.

Substituting  $g = \Delta v \delta(\tau - \tau_s)$  in Eq. (5) and integrating twice, we get

$$\begin{aligned} \eta_i(\tau) = & \eta_i(0) + \dot{\eta}_i(0)\tau \\ & + \Delta v \sum_{l=1}^{N-1} \sum_{j=1}^{N-1} \Gamma_l^2 W(i,l)W^{-1}(l,j) \\ & \times [ \eta_j(0) + \dot{\eta}_j(0)\tau_s ] (\tau - \tau_s) \Theta(\tau - \tau_s). \end{aligned} \quad (6)$$

Before considering special cases and applications of Eq. (6) we note a few points. As in Eq. (4) we see that all the modes, indicated by the summation over  $l$ , contribute to the time evolution of  $\eta_i(\tau)$  at each interface  $i = 1, 2, \dots, N-1$ . Similarly, the initial conditions at all the interfaces, indicated by the summation over  $j$ , contribute to  $\eta_i(\tau)$ . Note that since  $\eta_j(0) + \dot{\eta}_j(0)\tau_s = \eta_j(\tau_s)$ , it is actually the instantaneous values of  $\eta_j$  at shock time  $\tau_s$  that influence  $\eta_i(\tau)$ .

As seen from Eq. (6), the effect of the shock is to change the rate of change  $d\eta_i/d\tau$ . The amplitude  $\eta_i$  itself is not immediately affected by the shock,  $\eta_i(\tau_{s+}) = \eta_i(\tau_{s-})$ , where  $\tau_{s\pm}$  refer to times immediately before and after the shock. The amplitude remains the same but its slope is changed suddenly so that  $\dot{\eta}_i(\tau_{s+}) \neq \dot{\eta}_i(\tau_{s-})$ .

We now consider special cases of Eq. (6) which illustrate the above remarks and also have interesting properties.

## III. SPECIAL CASES

### A. $N=2$

This is the classical case considered by Richtmyer.<sup>3</sup> The density profile is shown in Fig. 2(a). Since there is only

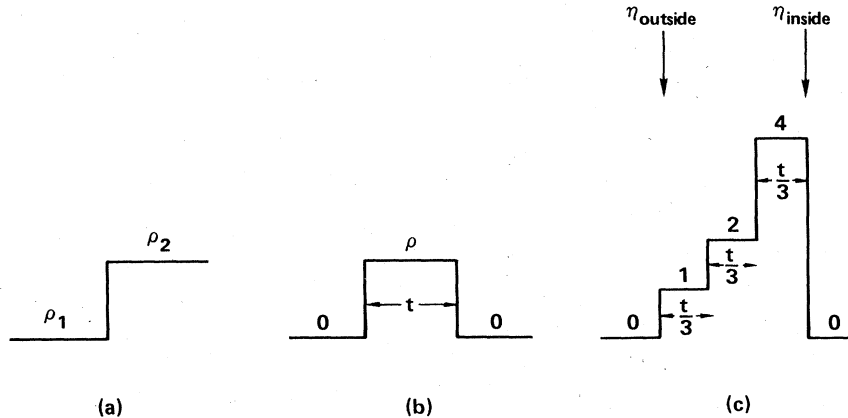


FIG. 2. (a) The density profile for the classical case  $N=2$  with one interface. (b) The density profile for  $N=3$  and for the special case  $\rho_1 = \rho_3 = 0$ ,  $\rho_2 = \rho$  and  $t_1 = t_3 = \infty$ ,  $t_2 = t$ . (c) The density profile for  $N=5$  with densities  $(0, 1, 2, 4, 0)$  and thicknesses  $(\infty, t/3, t/3, t/3, \infty)$ . The amplitudes  $\eta_{\text{outside}}$  and  $\eta_{\text{inside}}$  refer to perturbations at the first and last interfaces, respectively.

one interface and only one term in the sum indicated in Eq. (6), we drop the subscripts. Of course,

$$\Gamma^2 = \gamma_{\text{classical}}^2 / g = kA = k(\rho_2 - \rho_1) / (\rho_2 + \rho_1),$$

and we get

$$\begin{aligned} \eta(\tau) = & \eta(0) + \dot{\eta}(0)\tau \\ & + \Delta v k \left[ \frac{\rho_2 - \rho_1}{\rho_2 + \rho_1} \right] [\eta(0) + \dot{\eta}(0)\tau_s] \\ & \times (\tau - \tau_s) \Theta(\tau - \tau_s). \end{aligned} \quad (7)$$

We are considering a system of two semi-infinite fluids moving under the action of an isolated shock; between  $\tau=0$  and  $\tau=\tau_s$  the system is coasting at some constant velocity  $v(0)$ . At  $\tau=\tau_s$  a shock induces a jump velocity  $\Delta v$  and after  $\tau=\tau_s$  the system coasts with velocity  $v(0) + \Delta v$ . The jump occurs instantaneously at  $\tau=\tau_s$ . Perturbations at the interface, which may have been increasing or decreasing linearly with time until  $\tau=\tau_s$ , continue to evolve linearly in time but with a new slope given by  $\dot{\eta}(0) + \Delta v k A \eta(\tau_s)$ . If the initial conditions read  $\dot{\eta}(0) = \tau_s = 0$ , then

$$\eta(\tau) / \eta(0) = 1 + \Delta v k A \tau, \quad (8)$$

(RM case) which agrees with the result derived in Ref. 3.

It is clear from Eq. (8) that, following a shock, perturbation amplitudes can increase or decrease depending on the sign of  $\Delta v A$ . If the shock proceeds from low to high density ( $\Delta v A > 0$ ), then perturbations increase, while a shock proceeding from high to low density ( $\Delta v A < 0$ ) causes perturbations to decrease. However, if the system continues to coast, perturbations in the second case simply go through zero, i.e., change phase, and continue to grow in absolute magnitude.

For the RT case of constant acceleration  $g$ , Eq. (8) is replaced by

$$\eta(\tau) / \eta(0) = \cosh(\sqrt{kgA} \tau), \quad (9)$$

(RT case) again assuming  $\dot{\eta}(0) = 0$ . For  $gA < 0$ , i.e., high-density fluid accelerating low-density fluid, the system is stable and  $\eta(\tau)$  oscillates in time and never grows any larger than its initial value as long as the system continues to accelerate in the same direction. We conclude that while the distinction between stable and unstable cases  $gA < 0$  and  $gA > 0$  is clear for RT instabilities, that distinction becomes somewhat blurred for RM instabilities where perturbations grow in magnitude for both cases  $\Delta v A > 0$  and  $\Delta v A < 0$ .

We now take advantage of Eq. (7), which is general and accommodates arbitrary initial conditions, to analyze all possible cases of how  $\eta(\tau)$  can evolve after the passage of a shock at  $\tau=\tau_s$ . There are 15 possibilities, not all of which are allowed for a given sign of  $\Delta v A$ . These are shown in Fig. 3. For a "stable" shock, i.e.,  $\Delta v A < 0$ , Figs. 3(a)–3(i) are allowed while the rest are not allowed. For an "unstable" shock, i.e.,  $\Delta v A > 0$ , only Figs. 3(i)–3(o) are allowed. The two simplest cases with  $\dot{\eta}(0) = 0$  are shown in Figs. 3(a) and 3(j); the rest are obtained by con-

sidering a positive or negative  $\dot{\eta}(0)$  and short or long shock arrival time  $\tau_s$ . One may imagine, for example, that the initial conditions were set by a first shock at  $\tau=0$  and the perturbations evolve until a second shock arrives at  $\tau=\tau_s$ . The effect of this second shock is to change  $\dot{\eta}$  by an amount equal to  $\Delta v k A \eta(\tau_s)$ .

We will discuss only a few out of the 15 cases shown in Fig. 3. Figure 3(i) is the case  $\eta(\tau_s) = 0$  in which case neither a stable shock nor an unstable shock has any effect on the perturbation. Of course, this happens if the second shock is timed to arrive exactly at  $\tau_s = -\eta(0) / \dot{\eta}(0)$ .

Perhaps the more interesting cases are shown in Figs. 3(c), 3(g), and 3(n), where the amplitude is "frozen out" and remains constant after the shock. Obviously this is achieved when the slope change caused by the second shock exactly cancels the slope set by the previous one. Timing must be such that the interval time between the two shocks is

$$\tau_s^* = - \frac{\dot{\eta}(0) + \Delta v k A \eta(0)}{\Delta v k A \dot{\eta}(0)}. \quad (10)$$

It is interesting to point out that this freezing out of the amplitude can be achieved with a stable shock ( $\Delta v A < 0$ ) in both cases of  $\dot{\eta}(0) > 0$  or  $\dot{\eta}(0) < 0$ , as indicated in Figs. 3(c) and 3(g), while an unstable shock ( $\Delta v A > 0$ ) can freeze out an amplitude only if it previously was decreasing, i.e.,  $\dot{\eta}(0) < 0$ , as indicated in Fig. 3(n).

Freezing out can be used as a stabilizing mechanism particularly for perturbations on the inside of inertial-confinement-fusion (ICF) shells where the shocks are stable as they proceed into the fuel. Of course real targets have perturbations in a range of wavelengths and, since the timing condition in Eq. (10) depends on  $k$ , one can completely freeze out perturbations of a given wavelength  $\lambda$ , while others close to  $\lambda$  will have reduced, but nonzero, growth rates.

Finally, we point out that it is, unfortunately, impossible to freeze out an amplitude as it passes through zero.

#### B. $N=3$

The system consists of three fluid layers of densities  $\rho_1$ ,  $\rho_2$ , and  $\rho_3$ , with  $t_1 = t_3 = \infty$ . The eigenvalues and eigenfunctions for arbitrary densities were given previously<sup>6,7</sup> and will not be repeated here. Instead, we will consider the more specialized case of  $\rho_1 = \rho_3 = 0$ , i.e., a single fluid with two free boundaries as shown in Fig. 2(b).

As indicated in Fig. 2(b), we let  $\rho$  and  $t$  denote the density and thickness, respectively, of the "middle" layer ( $\rho_2 = \rho$  and  $t_2 = t$ ). The results are independent of  $\rho$  since the eigenvalue equation, Eq. (3), involves only the ratios of densities. Furthermore,  $t$  appears only in the combination  $kt$ .

The two eigenvalues are  $\Gamma_1^2 = -\Gamma_2^2 = k$ , and the eigenfunctions are  $W(1,1) = W(2,2) = 1$ ,  $W(1,2) = W(2,1) = e^{-kt}$ . The elements of the inverse matrix  $W^{-1}$  are

$$\begin{aligned} W^{-1}(1,1) = W^{-1}(2,2) &= \frac{1}{1 - e^{-2kt}}, \\ W^{-1}(1,2) = W^{-1}(2,1) &= - \frac{e^{-kt}}{1 - e^{-2kt}}. \end{aligned} \quad (11)$$

Substituting these expressions in Eq. (6) we obtain

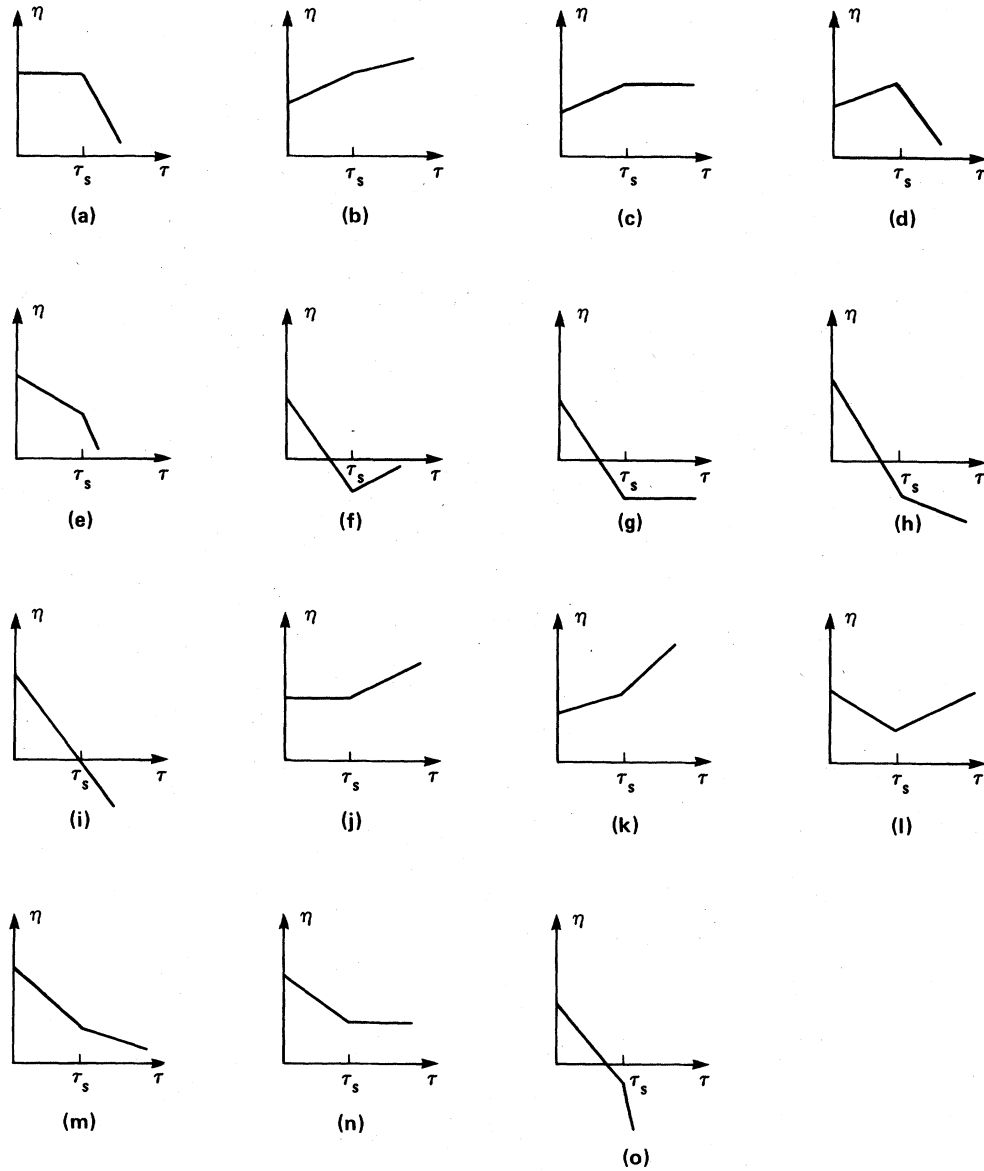


FIG. 3. Possible evolution patterns of the amplitude for the classical case  $N=2$ .  $\eta$  is the amplitude of perturbations at the interface between  $\rho_1$  and  $\rho_2$  [see Fig. 2(a)]. The system is assumed to be coasting until time  $\tau_s$ , at which time a shock induces a jump velocity  $\Delta v$ . Only diagrams (a)–(i) are allowed if the shock proceeds from a high to a low density. In the opposite case where the shock proceeds from a low to a high density, only diagrams (i)–(o) are allowed. It is possible to freeze out an amplitude as indicated in diagrams (c), (g), and (n).

$$\eta_1(\tau) = \eta_1(0) + \dot{\eta}_1(0)\tau + \frac{\Delta v k}{1 - e^{-2kt}} \left\{ (1 + e^{-2kt})[\eta_1(0) + \dot{\eta}_1(0)\tau_s] - 2e^{-kt}[\eta_2(0) + \dot{\eta}_2(0)\tau_s] \right\} (\tau - \tau_s)\Theta(\tau - \tau_s), \quad (12)$$

$$\eta_2(\tau) = \eta_2(0) + \dot{\eta}_2(0)\tau - \frac{\Delta v k}{1 - e^{-2kt}} \left\{ (1 + e^{-2kt})[\eta_2(0) + \dot{\eta}_2(0)\tau_s] - 2e^{-kt}[\eta_1(0) + \dot{\eta}_1(0)\tau_s] \right\} (\tau - \tau_s)\Theta(\tau - \tau_s). \quad (13)$$

Clearly,  $\eta_2(\tau) = \eta_1(\tau)$  with  $1 \leftrightarrow 2$  and  $\Delta v \rightarrow -\Delta v$ . Our convention is that a positive  $\Delta v$  indicates a shock directed from  $\rho_1$  to  $\rho_2$ .

At short wavelengths  $\lambda$  or, equivalently, at large thicknesses  $t$ , i.e.,  $kt \gg 1$ , the two interfaces decouple and the two equations (12) and (13) each reduce to Eq. (7) with

an Atwood number of  $\pm 1$ . In the opposite limit of long wavelength or small thickness  $t$ , i.e.,  $kt \ll 1$ , the two interfaces "see" each other and the evolution at one interface depends very much on the other.

Let us consider the case  $\dot{\eta}_1(0) = \dot{\eta}_2(0) = \eta_2(0) = \tau_s = 0$ . The system is shown in Fig. 4. Initially only one of the

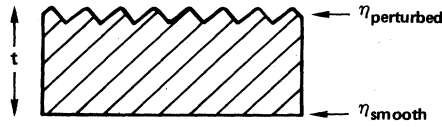


FIG. 4. The simplest case for  $N=3$ : a fluid layer of density  $\rho$  and thickness  $t$  having two free boundaries [see Fig. 2(b)]. Initially one surface is perturbed while the other is perfectly smooth. Perturbations at each surface evolve according to Eqs. (14) and (15).

free surfaces is perturbed with amplitude  $\eta_0$ , while the other surface is perfectly smooth. Then,

$$\frac{\eta_{\text{perturbed}}}{\eta_0} = 1 + \frac{\Delta v k}{1 - e^{-2kt}} (1 + e^{-2kt}) \tau, \quad (14)$$

$$\frac{\eta_{\text{smooth}}}{\eta_0} = 2 \frac{\Delta v k e^{-kt}}{1 - e^{-2kt}} \tau. \quad (15)$$

For the case of RT instability, the corresponding equations are

$$\frac{\eta_{\text{perturbed}}}{\eta_0} = \frac{1}{1 - e^{-2kt}} [\cosh(\sqrt{gk} \tau) - e^{-2kt} \cos(\sqrt{gk} \tau)], \quad (16)$$

$$\frac{\eta_{\text{smooth}}}{\eta_0} = \frac{e^{-kt}}{1 - e^{-2kt}} [\cosh(\sqrt{gk} \tau) - \cos(\sqrt{gk} \tau)]. \quad (17)$$

Equations (14)–(17) illustrate how an initial perturbation at one interface can induce perturbations at the other interface.

#### IV. APPLICATIONS

In this section we will illustrate the numerical application of our technique with the case  $N=5$ . We have also treated problems with large  $N$  which are better approximations of density profiles in an imploding capsule. The results for the relatively long wavelengths considered here are not too sensitive to how well the density gradients are resolved, and the conclusions presented in this paper apply also to the cases with large  $N$ .

We now turn to a specific example. The densities are  $(0, 1, 2, 4, 0)$  and the thicknesses are  $(\infty, t/3, t/3, t/3, \infty)$ . This density profile is shown in Fig. 2(c). It was chosen for two reasons. First, it is representative of the density profile in ICF capsules where a shell of thickness  $t$  is driven from one side by low-density plasma and compresses low-density fuel on the other side. With this picture in mind, we will call the first interface, between  $\rho=0$  and  $\rho=1$ , the “outer surface” of the shell, and the last interface, between  $\rho=4$  and  $0$ , will be called the “inner surface.” The reader must keep in mind that the geometry assumed in all our calculations is planar (see Fig. 1) and not spherical as suggested by the terms inner and outer.

The second reason for choosing this admittedly simple density profile is that we can obtain analytic expressions

for its four eigenvalues. Two of the eigenvalues are given by  $\gamma^2/gk = +1$  and  $-1$ , and the other two are

$$\frac{\gamma^2}{gk} = \frac{S(1+ST)(R^2-1) \pm S|R-1|\sqrt{R}}{R^2+R+1+S^2(R+1)^2}, \quad (18)$$

where  $S = \sinh(kt/3)$  and  $T = \tanh(kt/6)$ , and  $R$  is the common ratio of densities  $R = \rho_4/\rho_3 = \rho_3/\rho_2$  which is equal to 2 for the density profile shown in Fig. 2(c). We used these equations as a check of our numerical calculation.

We have not specified the units for the densities since an overall scale is immaterial. The density profile  $(0, 1, 2, 4, 0)$  is equivalent, for example, to  $(0, 3, 6, 12, 0)$ .

For the wavelength we chose  $\lambda = 3t$ . Several considerations led to this choice. As expected, very long ( $\lambda \gg t$ ) wavelength perturbations grow too slowly, while very short ( $\lambda \ll t$ ) wavelength perturbations grow very fast. For reasonable assumptions on surface finish, as discussed below, the very short wavelength perturbations grow so large that they are well outside the linear regime where our theory is applicable. Furthermore, the time evolution of very short wavelength perturbations is given to a good degree of accuracy by the classical expressions, Eqs. (1) and (2), applied at each interface independently. The interaction among the various interfaces, which is the main feature of our approach, becomes dominant at relatively longer wavelengths.

For our initial conditions we chose  $\dot{\eta}_1(0) = \dot{\eta}_2(0) = \dot{\eta}_3(0) = \dot{\eta}_4(0) = 0$ ,  $\eta_2(0) = \eta_3(0) = 0$ , and  $\eta_1(0) \equiv \eta_{\text{outside}}(0) = \eta_4(0) \equiv \eta_{\text{inside}}(0) = \eta(0)$ , that is, we chose to start with no perturbation within the fluids and with equally rough initial surface finish  $\eta(0)$  on the inside and outside surfaces. As the surface perturbations  $\eta_1$  and  $\eta_4$  evolve in time, the fluid develops internal perturbations, i.e.,  $\eta_2$  and  $\eta_3$  grow from their initial zero value to rather large values as they are driven by the surface perturbations.

We considered five different velocity histories shown as diagram (a) in Figs. 5–9. They are combinations of shocks and constant accelerations. In all cases we assumed that a final shock at  $\tau=5$  brings the shell to rest ( $v=0$ ), though, of course, in a capsule the shell would slow down, turn around, and move out. Our velocity histories represent fuel burn at about  $\tau \approx 5$ , though we will continue to evolve our equations up to  $\tau=6$  to show the effect of a large shock which proceeds from inside to the outside.

Our unit of length is set by  $t=1$ . The units of time are arbitrary. In Figs. 5–9 negative velocity indicates motion directed “inward,” i.e., from  $\rho=1$  to 4. An example will clarify these points. A shell  $10 \mu\text{m}$  thick with perturbation of  $\lambda = 30 \mu\text{m}$  on its outer and inner surfaces is stationary at  $\tau=0$ . Assume that it moves according to Fig. 6(a), and that time is measured in nanoseconds. Then at  $\tau=1$  ns the shell jumps inward with speed  $20 \mu\text{m/ns}$  and immediately afterwards accelerates inward with  $|g| = 20 \mu\text{m/ns}^2$  until  $\tau=4$  ns, at which time it is moving inward at  $80 \mu\text{m/ns}$ . We will call this maximum speed its “implosion velocity.” At  $\tau=4$  ns the shell decelerates with  $|g| = 30 \mu\text{m/ns}^2$  until  $\tau=5$  by which time its speed is reduced to  $50 \mu\text{m/ns}$ . A shock at  $\tau=5$  ns brings the

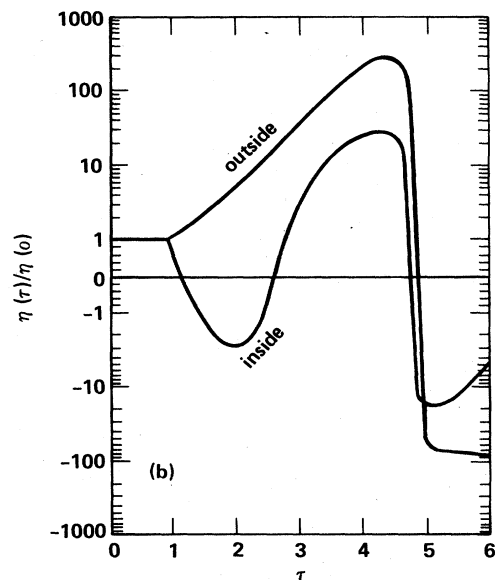
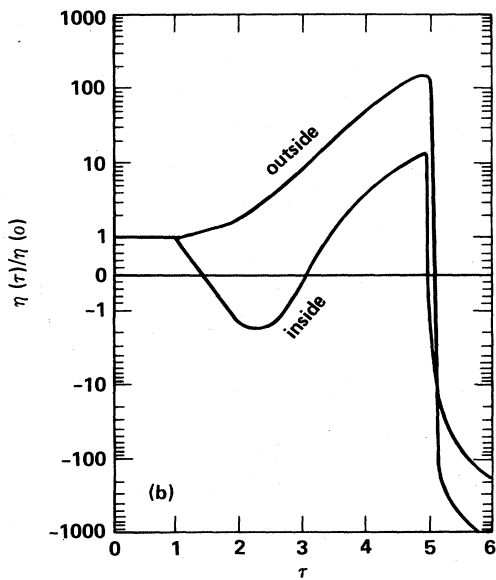
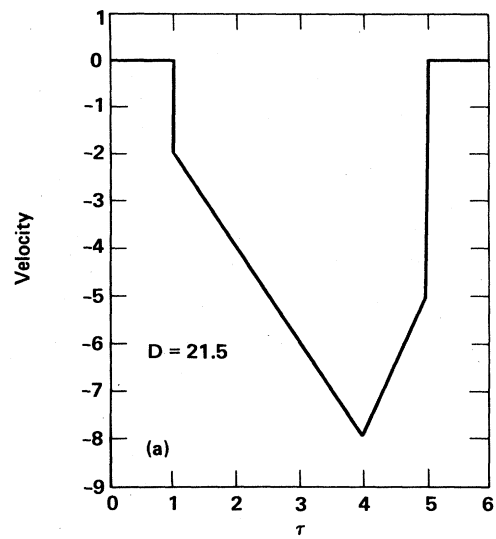
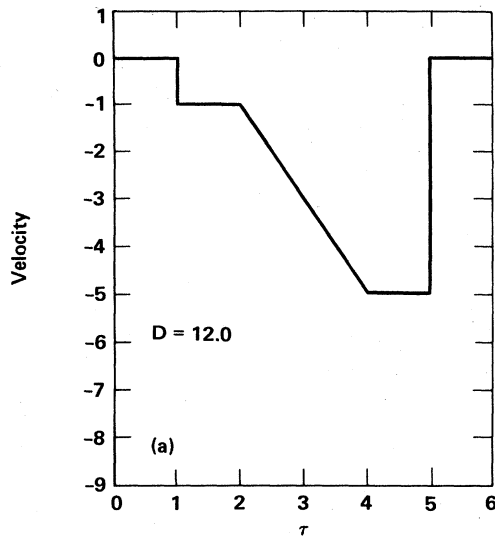


FIG. 5. (a) A velocity history describing the motion of a shell whose density profile is shown in Fig. 2(c). Negative velocities are directed from outside to inside. The shell thickness  $t$  is chosen as scale for length or distance. Units of time  $\tau$  are arbitrary.  $D = \int_0^6 v d\tau$ . In this case the shell covers a distance  $D$  of 12.0 times its thickness. (b) Evolution of perturbations at the outer and inner surfaces of the shell, assuming the velocity history of diagram (a). Initially the outer and inner surfaces have perturbations of amplitudes  $\eta(0)$  and wavelengths  $\lambda = 3t$ .

FIG. 6. Same as Fig. 5 for a different velocity history. The system covers a distance of 21.5 times the shell thickness.

shell to rest; it has covered a total distance of 215  $\mu\text{m}$ .

The results of our calculations corresponding to the velocity histories of Figs. 5(a)–9(a) are shown in Figs. 5(b)–9(b), respectively. In these figures we show  $\eta_1(\tau)/\eta(0)$  and  $\eta_4(\tau)/\eta(0)$ , the “outside” and “inside” perturbations, as functions of time  $\tau$ .

The coupling between interfaces is most clear at  $\tau = 5$ , by which time the outer perturbation grows very large and “takes over”: the phase reversal of this outer perturbation immediately after the last shock (which brings the system to rest) is expected on classical grounds, since the shock, directed from inside out, proceeds from a high ( $\rho = 1$ ) to low ( $\rho = 0$ ) density at the outer surface. What is difficult to explain is the phase reversal at the *inner* surface where the shock proceeds from low density ( $\rho = 0$ ) to high density ( $\rho = 4$ ). This phase reversal can be understood if we remember that by this time the large outer perturbation

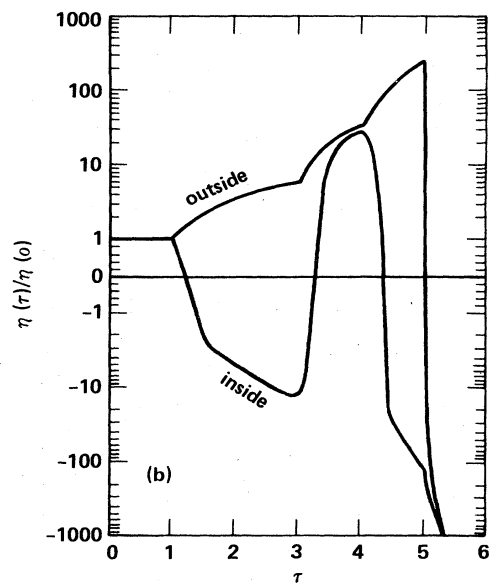
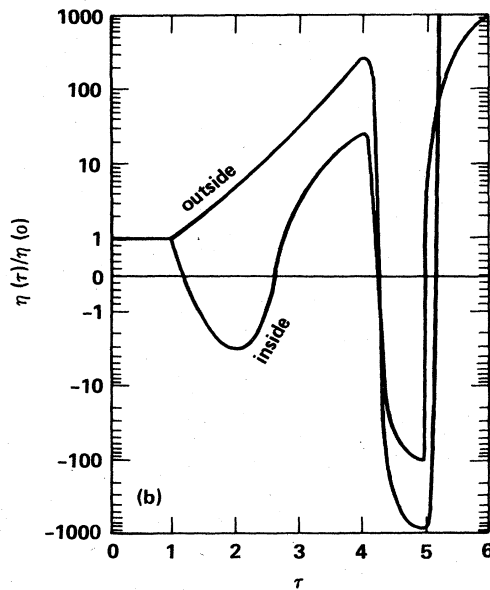
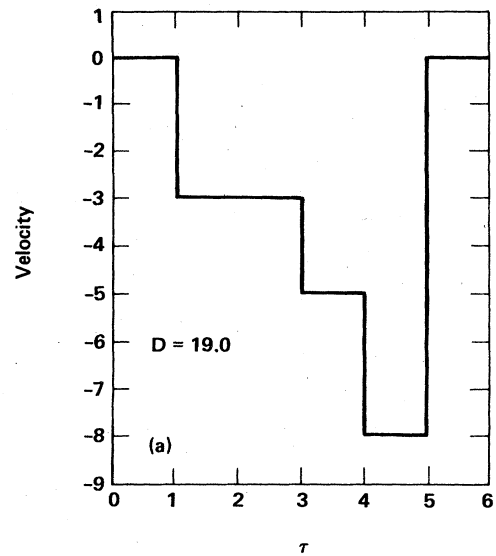
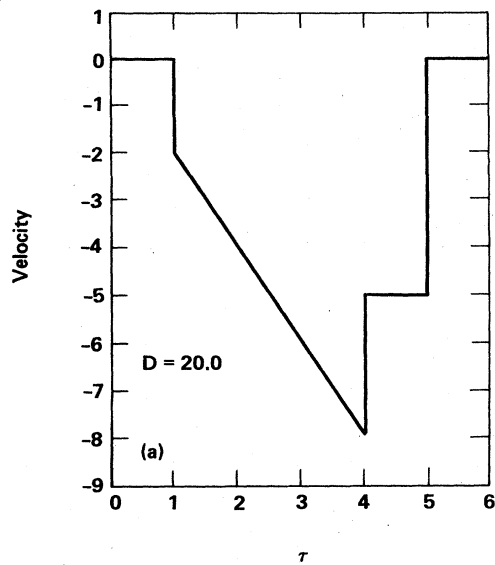


FIG. 7. Same as Fig. 5 for a different velocity history. The distance covered is 20.0 times the shell thickness.

FIG. 8. Same as Fig. 5 for a different velocity history consisting entirely of shocks. The distance covered is 19.0 times the shell thickness.

controls the rest of the perturbations; in other words, the inner perturbations reverse their phase because the outer perturbations have.

Figures 5–9 show that by  $\tau \approx 5$  perturbations have increased almost by a factor of about  $10^3$ . As mentioned earlier, shorter wavelength perturbations grew even more, particularly on the outer surface, and our choice of  $\lambda = 3t$  was partly motivated by reasonable estimates of surface finish and how much growth can be tolerated because our calculation breaks down when  $\eta_1 > \lambda$  and nonlinear effects

come into play. Going back to our example of a shell 10  $\mu\text{m}$  thick, it is reasonable to assume an initial surface finish of  $\eta(0) \gtrsim 100 \text{ \AA}$ . Growing a thousandfold this amplitude reaches  $\eta \gtrsim 10 \mu\text{m}$  and is barely within the linear regime since  $\lambda = 30 \mu\text{m}$ . Clearly, choosing a shorter wavelength which grows faster would have taken us well beyond the linear regime and the validity of our theory unless, of course, we assumed a much smaller initial amplitude.

In Figs. 5–9 three out of the four inputs are kept fixed

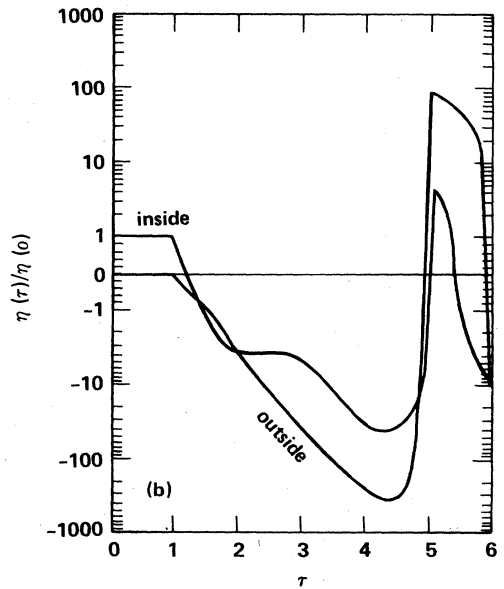
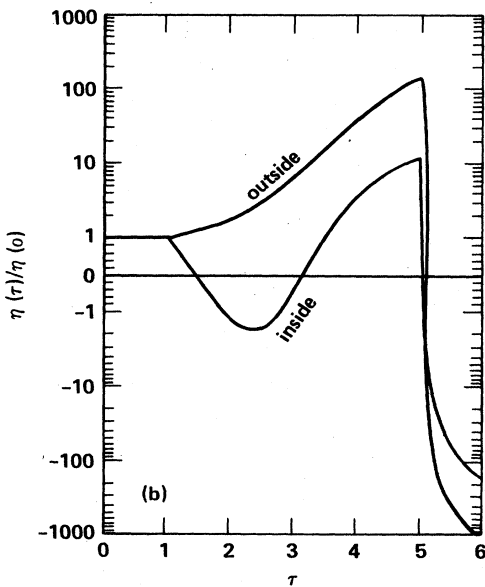
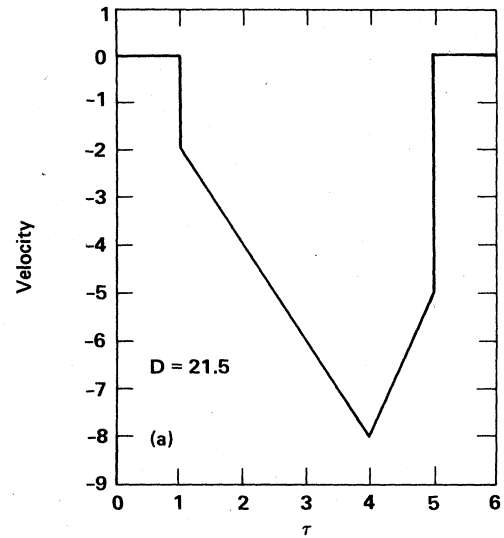
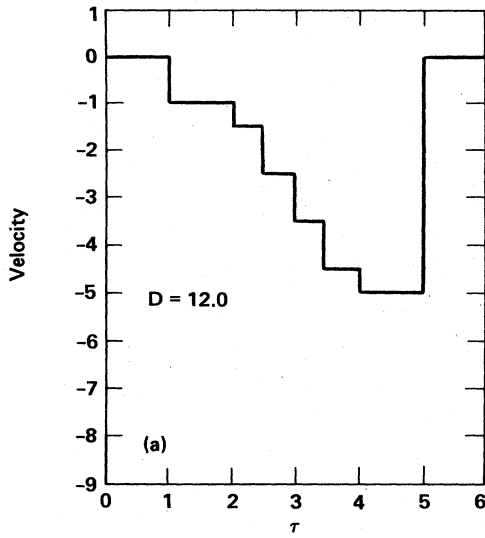


FIG. 9. Same as Fig. 5 for a velocity history similar to Fig. 5(a) in which the constant acceleration between  $\tau=2$  and  $\tau=4$  is replaced by a series of five small shocks. Compare with Fig. 5.

FIG. 10. Same as Fig. 6 but with different initial conditions: only the inner surface has initial perturbations; the outer surface starts perfectly smooth. Compare with Fig. 6.

(same density profile, same wavelength, and same initial conditions on the  $\eta_i$ ). Only the fourth input, viz., the velocity history, is varied in Figs. 5–9. The growth of the perturbations clearly depends on the velocity history of the shell, as these figures illustrate.

Finally, we show an example of how a perfectly smooth outer surface develops perturbations as large as the case of an initially rough outer surface. In Fig. 10 we show how

perturbations evolve from the initial values  $\eta_{\text{outside}}(0)=0$  and  $\eta_{\text{inside}}=\eta(0)$ , i.e., all surfaces start perfectly smooth except for the inside surface. The velocity history is that of Fig. 6(a). Comparing Figs. 6(b) and 10(b) we see that an initially smooth outer surface does not necessarily suppress the growth of perturbations at later times—a perturbation at only one interface can act as seed for perturbations throughout the fluid.

### V. COMMENTS AND CONCLUSIONS

(i) We ran a number of tests to check the code: First, at short wavelengths the interfaces decouple because the off-diagonal matrix elements of  $M$  in Eq. (3) go to zero like  $1/\sinh(kt_i)$ , and the results agree with the classical expressions. Second, for  $N=3$  the code gives the same results as in Eqs. (12) and (13) for the case  $\rho_1=\rho_3=0$ . Third, the four eigenvalues calculated by the code for the density profile shown in Fig. 2(c) and for  $\lambda=3t$  are  $\gamma/\sqrt{g}=1.447, 0.821, 0.553,$  and  $1.447i$ ; these numbers agree very closely with the expressions given in the previous section [see Eq. (18) and the discussion preceding it]. Finally, Figs. 5 and 9 show that if the velocity histories are sufficiently similar, then the perturbations evolve similarly. In fact, Fig. 9 was run just to check if a series of small shocks can imitate a constant acceleration: the velocity history shown in Fig. 5(a) is a combination of shocks and accelerations, hence the perturbations were evolved using both Eqs. (4) and (6), while the velocity history of Fig. 9(a) consists entirely of shocks and is similar to Fig. 5(a) except that the constant acceleration between  $\tau=2$  and 4 is replaced by a number of small shocks. Hence only Eq. (6) is used to evolve the perturbations, and the result, shown in Fig. 9(b), is quite similar to Fig. 5(b).

Clearly, an acceleration history that varies continuously with time can also be treated in this fashion by breaking it down into a series of small shocks and constant accelerations and using the appropriate equation in each time step.

(ii) Before applying our techniques to an actual system, one must of course check if the assumptions of linearity, incompressibility, no heat transfer, no viscosity, and no surface tension are satisfied. The examples treated in the previous section were inspired from ICF implosions. A number of complex processes are involved, and no doubt our techniques will never replace full 2D hydrodynamic calculations of the Rayleigh-Taylor instability as reported in the literature.<sup>8</sup>

For ICF implosions, while surface tension and viscosity are practically absent, realistic initial amplitudes can quickly evolve into the nonlinear regime where our equations break down. Furthermore, we cannot justify the assumption of no heat transfer in ICF capsules since the shells are driven by ablation. A number of calculations<sup>9,8</sup> indicate that ablation reduces the growth rates for Rayleigh-Taylor instabilities, in which case we would be overestimating the growth at the outer surface. This would have important consequences since, as discussed in the previous section, the inner perturbations are driven

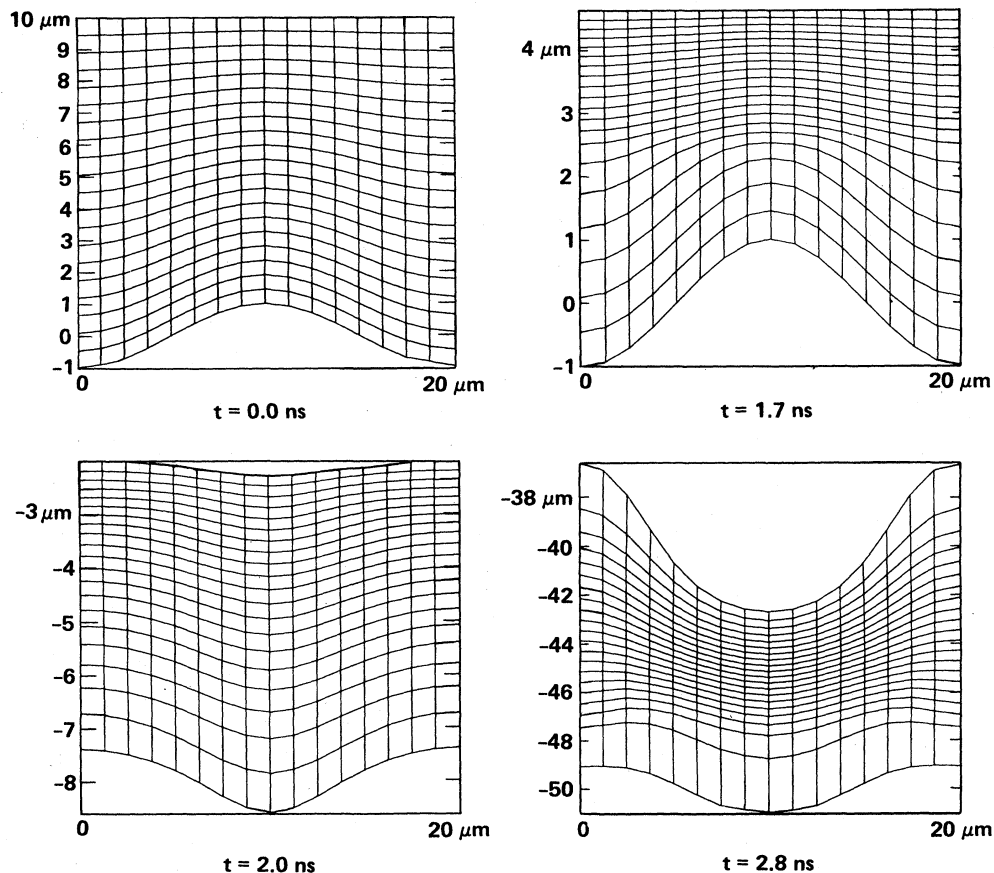


FIG. 11. Snapshots of the lower half of a 20- $\mu\text{m}$ -thick glass target driven by ablation (see text). The perturbation has a wavelength of 20  $\mu\text{m}$  and an initial amplitude of 1  $\mu\text{m}$ . The perturbation starts at the backside, changes phase after the passage of the shock, and later feeds through to the ablation surface. The code is Lagrangian in the direction of motion, so that each snapshot shows the same fluid at different times.

largely by the growth of the outer perturbations. If a mechanism stabilizes the outer surface, then we have reason to expect that the inner perturbations also will not grow very large. We must point out, however, that other 2D hydrodynamic calculations<sup>10</sup> do not show a reduction in the growth rate and that there is no clear experimental evidence for such stabilization.

We have carried out a few 2D hydrodynamic calculations with targets driven by ablation and find that the effect depends on the target material. Of course, material properties and the effects of ablation are completely absent from the analytic theory presented in this paper; however, other characteristics of our theory, specifically feed through of long wavelength perturbations from one surface to another and phase reversal of amplitudes when shocks proceed from a high- to a low-density fluid were found in our 2D calculations also.

We illustrate with a problem run on the 2D hydrodynamic code LASNEX.<sup>11</sup> The target is 20- $\mu\text{m}$ -thick  $\text{SiO}_2$  glass with perturbations of wavelength  $\lambda=20\ \mu\text{m}$  and initial amplitude  $\eta(0)=1\ \mu\text{m}$  on its backside, i.e., away from the ablation surface. In Fig. 11 we show snapshots of the lower half of the fluid at  $t=0$ , 1.7 ns, 2.0 ns, and 2.8 ns. The drive corresponds to an about 10-kJ laser pulse whose full width at half maximum, peak power occurring at about 2.0 ns. By  $t=1.7$  ns we see that the lower half of the glass has been compressed by a factor of 2 from its initial 10  $\mu\text{m}$  thickness to about 5  $\mu\text{m}$ . At this time the shock is about 2  $\mu\text{m}$  away from the backside. At  $t=2.0$  ns the shock has broken through and the amplitude has reversed its phase. The target begins to accelerate and by  $t=2.8$  ns it covers a distance of about 50  $\mu\text{m}$ . Also, by 2.8 ns the upper half of the glass (not shown) has ablated away so that only the lower half is still dense. The ablation surface, as shown in Fig. 11, exhibits rather large perturbations, about 6  $\mu\text{m}$  peak to valley, induced by perturbations feeding through from the backside to the ablation surface. Perturbations continue to grow after 2.8 ns.

(iii) Finally, we discuss the assumption of incompressibility. For the case of the Rayleigh-Taylor instability it is not yet clear whether the effect of compressibility is to cause an increase or decrease in the growth rate (see Ref. 12). In the case of the Richtmyer-Meshkov instability the

effects of compressibility would be even more important, since real fluids invariably get compressed upon the passage of a shock.

Given the assumptions that go into the derivation of the classical expression

$$\frac{d\eta}{d\tau} = \eta \Delta v k \frac{\rho_2 - \rho_1}{\rho_2 + \rho_1}, \quad (19)$$

it is indeed surprising that experiments and numerical calculations with compressible fluids gave results consistent with it: Richtmyer's numerical calculations<sup>3</sup> were consistent with Eq. (19) provided he used the postshock, i.e., compressed amplitude and the postshock densities in this equation. He considered a shock proceeding from a light to a heavy fluid. Subsequent numerical calculations by Meyer and Blewett<sup>13</sup> agreed with Richtmyer's results and, for the case of a shock proceeding from a heavy to a light fluid, they suggested using the average of preshock and postshock amplitudes in Eq. (19). Experiments by Meshkov<sup>4</sup> were also consistent, within a factor of  $\sim 2$ , with Eq. (19) and confirmed the fact that perturbations grow linearly with time whether the shock proceeds from light to heavy or from heavy to light fluids.

Thus there is some evidence that the classical expression, in which a shock is treated as an impulsive acceleration, does a reasonably good job for the case  $N=2$ . Whether our extension to arbitrary  $N$  is also reasonable remains to be seen by new calculations and experiments.

*Note added in proof.* A recent experiment<sup>14</sup> has measured the growth of perturbations which initially start on the rear surface of a foil, i.e., opposite the side facing the laser.

#### ACKNOWLEDGMENTS

I am grateful to Gene Burke and Viviane Rupert for bringing the problem of shock-initiated instabilities to my attention. John Nuckolls and John Lindl have made valuable suggestions. This work was performed under the auspices of the U.S. Department of Energy by the Lawrence Livermore National Laboratory under Contract No. W-7405-ENG-48.

<sup>1</sup>Lord Rayleigh, *Scientific Papers* (Dover, New York, 1900), Vol. 2.

<sup>2</sup>G. I. Taylor, Proc. R. Soc. London, Ser. A 201, 192 (1950).

<sup>3</sup>R. D. Richtmyer, Commun. Pure Appl. Math. 13, 297 (1960).

<sup>4</sup>E. E. Meshkov, Izv. Akad. Nauk SSSR, Mekh. Zhidk. Gaza 5, 151 (1969).

<sup>5</sup>V. A. Andronov *et al.*, Zh. Eksp. Teor. Fiz. 71, 806 (1976) [Sov. Phys.—JETP 44, 424 (1976)].

<sup>6</sup>K. O. Mikaelian, Phys. Rev. Lett. 48, 1365 (1982); Phys. Rev. A 26, 2140 (1982).

<sup>7</sup>K. O. Mikaelian, Phys. Rev. A 28, 1637 (1983).

<sup>8</sup>R. L. McCrory, L. Montierth, R. L. Morse, and C. P. Verdon, Phys. Rev. Lett. 46, 336 (1981); M. H. Emery, J. H. Gardner, and J. P. Boris, *ibid.* 48, 677 (1982); R. G. Evans, A. J. Bennett, and G. J. Pert, *ibid.* 49, 1639 (1982).

<sup>9</sup>S. E. Bodner, Phys. Rev. Lett. 33, 761 (1974).

<sup>10</sup>J. D. Lindl and W. C. Mead, Phys. Rev. Lett. 34, 1273 (1975).

<sup>11</sup>G. B. Zimmerman, University of California Report No. UCRL-74811, 1973 (unpublished).

<sup>12</sup>I. B. Bernstein and D. L. Book, Phys. Fluids 26, 453 (1983).

<sup>13</sup>K. A. Meyer and P. J. Blewett, Phys. Fluids 15, 753 (1972).

<sup>14</sup>J. Grun *et al.*, Phys. Rev. Lett. 53, 1352 (1984).